Applied Catalysis B: Environmental 322 (2023) 122115

Contents lists available at ScienceDirect

Applied Catalysis B: Environmental

journal homepage: www.elsevier.com/locate/apcatb

Graphene quantum dots/NiTi layered double hydroxide heterojunction as a highly efficient De-NOx photocatalyst with long persistent post-illumination action

Javier Fragoso [a], Adrián Pastor [a,*,1], Manuel Cruz-Yusta [a], Francisco Martin [b], Gustavo de Miguel [c], Ivana Pavlovic [a], Mercedes Sánchez [a], Luis Sánchez [a,*,2]

[a] Departamento de Química Inorgánica, Instituto Químico para la Energía y Medioambiente IQUEMA, Universidad de Córdoba, Campus de Rabanales, E-14014 Córdoba, Spain
[b] Departamento de Ingeniería Química, Facultad de Ciencias, Universidad de Málaga, Campus de Teatinos, E-29071 Málaga, Spain
[c] Departamento de Química Física y Termodinámica Aplicada, Instituto Químico para la Energía y Medioambiente IQUEMA, Universidad de Córdoba, Campus de Rabanales, E-14014 Córdoba, Spain

ARTICLE INFO

Keywords:
Graphene
LDH
NOx
Persistent photocatalysis

ABSTRACT

Persistent photocatalysis is an attractive process to broaden the spectrum of environmental applications. Herein, blue luminescent graphene quantum dots (GQD) are incorporated into NiTi-based layered double hydroxide nanosheets (NiTi-LDH) by a facile impregnation method. The enhanced performance of GQD/NiTi-LDH leads to excellent NO photo-removal activity (61 %) and insignificant NO_2 release (< 0.6 %), beating the standard TiO_2 P25 (48 % and 14.2 %, respectively). Interestingly, after the end of light irradiation period, GQD/NiTi-LDH maintained a NO removal efficiency higher than 20 % for up to 75 min regardless of the previous irradiation time. This De-NOx post-photocatalytic process is the most effective reported at present. The dark/light mechanism is explained by the electron storage capacity of NiTi-LDH under light excitation, which is assisted by the electron migration from GQD to NiTi-LDH. Once the light is shut off, electrons are released and take part in the superoxide radical generation.

1. Introduction

The photocatalytic processes and related materials have been deeply studied as adequate environmental air remediation tools promoting the pollutant removal from the urban atmosphere [1]. The environmental photocatalytic air purification proceeds only under continuous external light irradiation source, this being the sunlight. Once light irradiation is absent, after sunset or because of the presence of clouds, the pollutant removal finishes immediately. Due to the high levels of atmospheric pollutants in geographical areas with large population, it is desirable that the removal of pollutants continue after sunset. This action is highly interesting for the removal of the NOx gases (De-NOx action) from the urban atmosphere. Nitrogen oxides, NOx (NOx = NO + NO_2), cause serious environmental problems and negative effects on human health [2]. The emission and accumulation of these gases in the urban atmosphere frequently exceed the limits recommended by international health institutions, this being a major concern for society [3]. Over the last two decades, high attention has been paid to the development of advanced photocatalysts, with successful results in terms of NOx removal and De-NOx selectivity under both UV and Visible light irradiation [4–6]. A typical curve of variations in NOx emissions for highly populated cities is shown in Fig. S1. It is observed that a main peak of NOx pollution occurs between 5 and 12.00 h. During this period, the photocatalytic process is useful for removing the pollutant gas. Of importance, the NOx concentration levels increase after the sunset, from 19 to 24 h. During this period the nitrogen oxide gases cannot be photocatalytically removed because of the absence of light irradiation. Therefore, it is highly interesting to develop new systems that allow the De-NOx process to be maintained once light irradiation is off, an action scarcely explored in this research field. To our knowledge, only few

* Corresponding authors.
E-mail addresses: q92paesa@uco.es (A. Pastor), luis-sanchez@uco.es (L. Sánchez).
[1] ORCID ID: 0000–0003-1115–0103
[2] ORCID ID: 0000-0002-0194-1908

https://doi.org/10.1016/j.apcatb.2022.122115
Received 27 June 2022; Received in revised form 10 October 2022; Accepted 25 October 2022
Available online 28 October 2022

works from T. Satoś research group have paid attention to the post-catalytical NOx removal in dark conditions [7–10].

Persistent Photo Catalysis (PPC) is a recent field of study aiming to sustain the photocatalytic processes once the light is off. In this sense, the development of post-photocatalytic reactions in the dark is assisted by two main processes: persistent luminescence and photo-assisted chemical reactions [11–13]. In the first case, materials with persistent luminescence (MPL) are mixed with photocatalytic materials (PCM) to prepare MPL@PCM composites. Basis on the storage capacity of the MPLs when they are illuminated for a short time, once the light is off, their correlated persistent luminescence is used by the PCM as a light source to sustain a self-induced photocatalytic activity in dark conditions. MPLs are mainly prepared by using rare earth elements as dopants, also being relevant the use of transition metal dopants (vg. Sr_2SiO_4:Eu^{2+} [14], $CaAl_2O_4$:Ce^{3+} [15], $Ca_6BaP_4O_{17}$:Eu^{2+} [16], $CaAl_2Si_2O_8$:Eu^{2+}, Dy^{3+} [17], $Ca_4(PO_4)_2O$:Eu^{2+},Y^{3+} [18], $MgAl_2Si_2O_8$:Mn^{4+} [19], $ZnGa_2O_4$:Cr^{3+} [20], Zn_2GeO_4:Mn^{2+} [21]). In the second case, the existence of an electron storage material (ESM) is required to allow the photocatalytic process to proceed under dark conditions. Basically, when the light source is on, the ESM is involved in the storage of electrons through the formation of an intermediate compound. In the absence of light this process is reverted, and electrons are released, sustaining the catalytic activity. Typical ESM materials are: TiO_2/WO_3 [22,23], $TiO_2/Ni(OH)_2$ [24], TiO_2/Cu_2O [25], Au-TiO_2/WO_3 [26], TiON/PdO [27], g-C_3N_4/CNTs/Gr [28], between others [12].

From the above, it is interesting to use PPC to enlarge the amount per day of NOx removed in the urban atmosphere. Satoś group proposed the use of MPL@PCM composites using $CaAl_2O_4$:(Eu,Nd) as MPL together with different photocatalytic materials such as $TiO_{2-x}N_y$, (Ta,N)-codoped TiO_2/Fe_2O_3, $SrTiO_3/Fe_2O_3$ or Cr-doped $SrTiO_3$ [7–10]. Once the light was off, post-photocatalytic De-NOx reactions during 100 – 180 min were observed for these materials. However, the NOx removal efficiency was as low as 8 – 10% and only a substantial abatement of NOx gases was accounted for during the first 15 mins in the dark. Since they are usually lower cost and easier to prepare than MPL materials, to enhance the post-photocatalytic De-NOx process in terms of efficiency and lifetime, we have studied the use of ESM materials.

In this work, we have successfully implemented the preparation of graphene quantum dots/layered double hydroxides as the first LDH-based heterojunction with a successful post-photocatalytic De-NOx response. Ni_3Ti-CO_3 layered double hydroxide (LDH) was selected because of its outstanding De-NOx ability (high NO conversion, outstanding selectivity and stable photocatalytic activity in running tests) [29]. In addition, it is known that some TiO_2-based heterojunctions lead to persistent photocatalysis. Specifically, the TiO_2/Cu_2O system has been demonstrated to photochemically works under dark conditions thanks to the prior accumulation of electrons in TiO_2 by Ti^{4+} partial reduction. This charge accumulation into TiO_2 comes from the electron injection from the Cu_2O phase under light conditions. Subsequently, the stored electrons are further released in the dark to promote photochemical reactions [25,30,31]. Similarly, the high dispersion of TiO_6 octahedra in NiTi-LDH and its pseudocapacitor properties might lead to these compounds acting as ESM [32,33]. On the other hand, the study of quantum dots (QDs) as a new type of light responsive 0D material with extraordinary applications in photocatalysis has flourished in the last decade [34–37]. Thus, the benefits of the use of carbon (CQDs) or graphene quantum dots (GQDs) in photocatalytic heterojunctions, specifically, enhanced photocatalytic activities (higher De-NOx efficiency) [38–42] and the potential luminescence light harvesting [43,44] were recently reported.

From the above premises, herein we propose the GQDs/Ni_3Ti-LDH compounds as new and efficient persistent De-NOx photocatalysts. We have prepared Ni_3Ti-CO_3 LDHs nanosheets by the Aqueous Miscible Organic Solvent Treatment (AMOST) [45], which were subsequently mixed with blue luminescent GQDs to form a 0D/2D heterojunction. A multi-technique characterisation enabled light to be shed on the physicochemical properties and the photocatalytic performance of the samples. We found that GQDs/Ni_3Ti compounds exhibit good photocatalytic NOx removal under UV and/or Visible light, and with a considerable persistence of the catalytic reaction in the dark. The persistent photocatalytic mechanism was explained on the basis of the results obtained by using EPR and DRIFTS techniques. The appealing post-photocatalytic De-NOx performance of the obtained materials opens the door to exploring LDHs compounds as new materials for persistent photocatalytic processes.

2. Experimental

2.1. Materials

$Ni(NO_3)_2{\cdot}6H_2O$, titanium isopropoxide (abbreviated as $Ti(O^iPr_4)$), Na_2CO_3, NaOH, HCl, $K_2Cr_2O_7$, p-benzoquinone (PBQ), Nafion™ 117 solution and 5,5-dimethyl-1-pyrroline-N-oxide (DMPO) were purchased from Sigma-Aldrich. Ethanol (EtOH; 99.8 %) and methanol (99.9 %) were purchased from PanReac AppliChem. Demineralised water was used in all the experiments. Blue luminescent graphene quantum dots (1 mg mL^{-1} in H_2O; abbreviated as GQDs) were purchased from Sigma-Aldrich, for which a complete characterisation is provided in Figs. S2. The measured Quantum Yield of the GQDs was 87 %.

2.2. Preparation of Ni_3Ti-CO_3 LDH nanosheets and GQDs/Ni_3Ti-LDH photocatalysts

The synthesis of Ni_3Ti-CO_3 LDH compound, labelled as NiTi-LDH, was carried out by the coprecipitation method following by the AMOST, as described in our previous work [29] and detailed in Supplementary Information (SI). The impregnation method was used to prepare photocatalysts containing GQDs with 1 wt% and 3 wt% of GQDs. For the first one, 0.3 g of NiTi-LDH nanosheets were placed in a glass petri dish (Ø = 40 mm) and 3 mL of GQD aqueous dispersion and 2 mL water were added. The slurry was stirred using a magnetic bar and heated to 50 °C to evaporate the solvent. Subsequently, 5 mL of EtOH were added while stirring and the solvent was allowed to evaporate at room temperature, the sample being collected and labelled as 1-GQDs/NiTi. To prepare the photocatalyst with 3 wt% of GQDs, 3-GQDs/NiTi sample, a similar procedure was carried out, but 9 mL of GQDs aqueous dispersion and 9 mL of EtOH were now used.

2.3. Characterisation and photocatalytic experiments

The structural, morphological, chemical identity and physical properties of the compounds were characterised by using different techniques: X-ray diffraction (XRD), X-ray photoelectron spectroscopy (XPS), Infra-red spectroscopy (IR), High-Resolution Transmission Electron Microscopy (HRTEM); thermogravimetric analysis (TGA), nitrogen adsorption–desorption isotherms study, ultraviolet-visible spectroscopy (UV-Vis), ultraviolet-visible diffuse reflectance spectroscopy (UV–vis DRS), steady-state photoluminescence (PL), time-resolved photoluminescence (TRPL), electron paramagnetic resonance (EPR), in situ diffuse reflectance infrared Fourier transform spectra (DRIFTS), ultraviolet photoelectron spectroscopy (UPS) and electrochemical measurements (Mott-Schottky). Additional detailed information about these studies is provided in “Supplementary Information” (SI).

The ISO 22197–1 method was used to carried out the NO gas abatement photocatalytic experiments. This is a method used to characterise the air purification measurement. The ability of the photocatalysts to induce NO photo-oxidation was assessed in a laminar flow reactor containing a 50 × 50 mm quartz sample holder with 300 mg of the powdered sample. The reactor was placed inside a solar simulator (Solarbox 3000e RH with Xe lamp; 36 and 250 W m^{-2} irradiances for UV and visible light, respectively). Experiments were also carried out under visible light irradiation by using a LED (λ = 420 nm; irradiance = 510 W

m^{-2}). De-NOx experiments were performed using NO gas (500 ppb; air balanced) as a reactant (flow rate gas = 0.37 L min^{-1}). The relative humidity was controlled to 50 ± 5 % by passing the air flow through a gas-washing bottle filled with demineralised water. Adsorption−desorption equilibrium for the photocatalysts was achieved after passing the air/NO flow in the dark for 10 min, before the irradiation period started. A photocatalytic blank test (empty sample holder) was carried out in order to discard NO photolysis. A chemiluminescence analyser (Environment AC32M) measured the concentration of NO, NO_x and NO_2 gases from the reactor outlet. Tests were repeated three times and the average concentration values were calculated. The obtained standard deviations were ~ 0.3 ppb for NO concentration and ~ 1.0 ppb for NO_2 and NO_x concentrations. The photocatalytic performance of the samples was studied regarding the NO, NO_x and selectivity (S) indexes:

$$NO\ conversion\ (\%) = \frac{([NO]_{in} - [NO]_{out})}{[NO]_{in}} \times 100$$

$$NOx\ conversion\ (\%) = \frac{([NO_x]_{in} - [NO_x]_{out})}{[NO_x]_{in}} \times 100$$

$$Selectivity;\ S\ (\%) = \frac{([NO_x]_{in} - [NO_x]_{out})/[NO_x]_{in}}{([NO]_{in} - [NO]_{out})/[NO]_{in}} \times 100$$

where $[NO]_{in}$, $[NO_X]_{in}$ and $[NO]_{out}$, $[NO_X]_{out}$ is the measured inlet and outlet concentrations, respectively, and $[NO_X] = [NO] + [NO_2]$.

3. Results and discussion

3.1. Composition and structural characterisation

The X-ray diffraction (XRD) patterns corresponding to NiTi-LDH and GQDs/NiTi samples are shown in Fig. 1a. These exhibit the characteristic reflections expected for a Ni_3Ti-CO_3 LDH prepared via the Aqueous Miscible Organic Solvent Treatment (AMOST procedure) [29]. The reflections for the (*003*) and (*006*) basal planes are located at 2θ ~ 10.9° and 22°, respectively, while the rest of the peaks at a higher 2θ angle correspond to (*012*), (*015*) and (*110*) planes[46]. The basal spacing d_{003} was calculated to be 8.09 Å, typical for a Ni_3Ti-AMO LDH and consistent with the presence of carbonate as the interlayer anion and the coexistence of ethanol molecules in the LDH gallery. During the AMOST procedure the organic solvent molecules replace the co-intercalated water molecules present in the interlayer galleries and, because the hydrogen bonding between layers is reduced [47], the LDH layer delamination is favoured and consequently layer stacking is reduced [45]. Thus, the basal XRD reflections were broad and low in intensity (Fig. 1a). On the other hand, the addition of GQDs during the AMOST procedure does not alter the LDH structure, as similar patterns were observed for GQDs/NiTi samples. Fig. 1b shows FT-IR spectra obtained for both samples. The intense and lower in frequency bands at 575 and 778 cm^{-1} correspond, respectively, to the M-O and HO-M-OH vibrational bending modes in the basal layer [48]. The vibration mode ν_3 of the CO_3^{2-} interlayer anions appears split into two bands at 1360 and 1483 cm^{-1}. The bending vibration of water molecules is observed at 1639 cm^{-1}, while the broad band at 3346 cm^{-1} shows the presence of O-H bonds. Noticeably, the low intensity signals at 1048, 2880 and 2982 cm^{-1} reveal the existence of ethanol molecules remaining adsorbed/incorporated in the LDH structure [29].

The chemical composition of the LDH sample was elucidated from TGA (Fig. S3a) and ICP-MS analysis. Good agreement was found between the experimental values and the theoretical metal ratios in the initial solution for a Ni_3Ti-LDH. The content of carbonate anions was assumed as those necessary to balance all the layer positive charge, and that for ethanol and water molecules (Fig. S3b) was calculated following the procedure previously reported for the Ni_3Ti-AMO LDH [29]. Thus, $[Ni_{0.77}Ti_{0.23}\ (OH)_2](CO_3)_{0.23}\ 0.16{\cdot}H_2O$ 0.1 EtOH is proposed as the chemical formula. The presence of graphene quantum dots in samples 1-GQDs/NiTi and 3-GQDs/NiTi was corroborated through photoluminescence experiments (Fig. S4), showing these samples blue fluorescence compared with NiTi-LDH sample under UV light (365 nm).

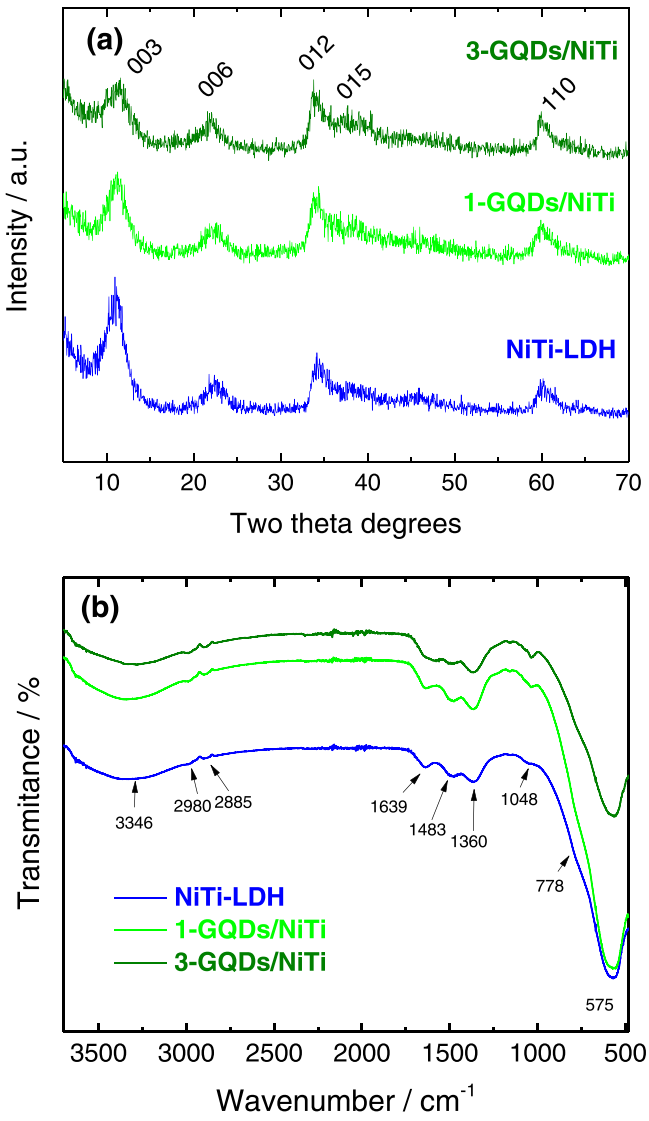

Fig. 1. (a) XRD patterns and (b) IR spectra obtained from the NiTi-LDH and GQDs/NiTi samples.

X-ray photoelectron spectroscopy (XPS) was used to analyse the oxidation states of Ti and Ni on the surface of NiTi-LDH and 3-GQDs/NiTi samples. Fig. 2 shows the XPS high resolution region of Ti2p, Ni2p, O1s and C1s. In order to ensure the correction of the energy shift, gold was used as a reference (Au $4f_{7/2}$ peak at 84.0 eV). The Ti2p photoelectron peak positions (Fig. 2a) for the NiTi-LDH sample ($Ti2p_{3/2}$ = 458.1 eV; $Ti2p_{1/2}$ = 463.9 eV) correspond to the contributions from Ti^{4+} ions in an octahedral coordination [29,49]. When GQDs are present in the sample, a shift to lower binding energies is observed for ($Ti2p_{3/2}$ = 457.8 eV; $Ti2p_{1/2}$ = 463.5 eV) which indicates the increased electron density on Ti atoms in LDH, suggesting the existence of chemical interactions between GQDs and NiTi. The binding energy for $Ni2p_{3/2}$ corresponds to hydroxide as corroborated by Warner's diagram [50], Fig. 2b. However, no changes were observed for Ni2p ($Ni2p_{3/2}$ = 855.2 eV; Fig. 2b) or NiLMM (843.3 eV kinetic energy) peaks recorded for both samples. This should be correlated with the difference in the 3d electron occupancy, Ti possesses empty states which could accept electrons from the HOMO levels of GQDs while Ni has the 3d orbitals

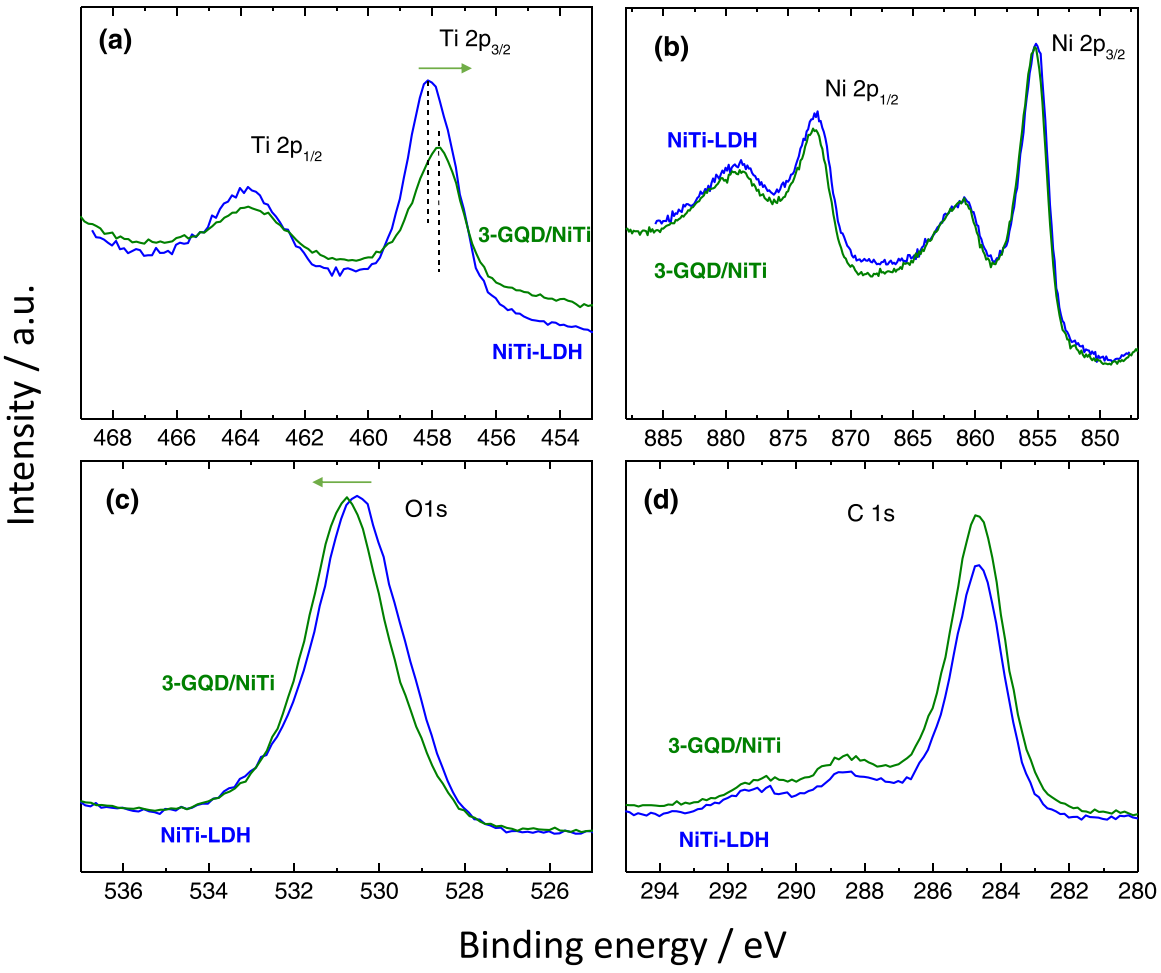

Fig. 2. XPS spectra obtained from the NiTi-LDH and GQDs/NiTi samples surface: (a) Ti 2p, (b) Ni 2p, (c) O 1 s and (d) C 1 s regions.

almost completely full [51]. The broad O1s peak is the result of different contributions: lattice oxygen in metal oxides, hydroxyl groups, carbonate, and adsorbed water. Due to the change in the electron density on Ti atoms in the 3-GQDs/NiTi sample, the O1s peak shifts to higher binding energy (530.8 eV) compared to the position recorded for the NiTi-LDH sample (530.5 eV), Fig. 2c. This result indicates that changes in electron density on metal atoms modify the spatial charge location in the layer [52]. Finally, the C1s photoelectron peaks (Fig. 2d) appear at 284.7, 288.5 and 291.1 eV, values corresponding to the adventitious carbon, carbonate and hydrocarbonate groups, respectively. The high intense signal of these adventitious species masks any information about C in GQDs, preventing to know about the changes in their electron density. However, the above XPS results demonstrate the occurrence of electronic interactions between GQDs and LDH, which should be beneficial for photocatalysis.

3.2. Morphology. Textural and optical properties

HRTEM study was performed to determine the morphology of the particles, Fig. 3. The NiTi-LDH sample appears as a two-dimensional solid (2D) and flower-type particles constituted by corrugated nanosheets, Fig. 3a. The 2D morphology is a consequence of the presence of ethanol molecules in the LDH structure, which displaces the water molecules from the interlayer space and reduces the hydrogen bonding tendency, the metal hydroxide layer exfoliation being promoted [53]. The observed thickness of the nanosheets is 1.5 – 3.0 nm (Fig. 3b), which means that they consist of a few LDH monolayers (Fig. 3c). After being modified with < 5 nm GQDs, the LDH maintains the original 2D morphology (Fig. S5a). In contrast to the pristine sample (Fig. S5b), the HRTEM image of GQDs/NiTi shows how GQDs are embedded in the nanosheets (Fig. S5c). The high-resolution TEM image of GQDs/NiTi reveals the hexagonal lattice with lattice interplanar spacing of 0.30 nm corresponding to the exposed (001) facets of the NiTi-LDH [54], Fig. 3d. In addition, lattice interplanar spacing of 0.21 nm belongs to the graphene quantum dots [41].

The BET surface area of photocatalysts were investigated by N_2 adsorption–desorption isotherms. Fig. 4a shows the isotherm corresponding to the NiTi-LDH sample, of which shape is a characteristic of a type IV isotherm with a H3 hysteresis loop. This pore structure, typical of LDHs, obtained by the AMOST method [29], corresponds to slit-shaped pores appearing from the nano-sheet morphology as observed in TEM images. A high specific surface area value of 410 m^2g^{-1} was estimated and related with the presence of mesoporous and macroporous pores, respectively (Fig. 4b). The preparation of GQDs/NiTi did not alter the pore structure nor the surface areas of the samples (Fig. S6) also exhibiting specific surface area values around 400 m^2g^{-1}. The mentioned features predict a good photochemical De-NOx response, as the contact with the reactant gas molecules and the photocatalyst́s active sites should be facilitated across the large area exposed.

The light absorption properties of the NiTi-LDH and GQDs/NiTi samples were inferred from their diffuse reflectance UV–Vis absorption spectra. Two sets of bands were observed (Fig. 4c), those with the highest intensity located at the 200 – 400 nm range are pertained to the ligand to-metal charge transfer for Ti(IV) cations in an octahedral environment. On the other hand, low intensity and broad bands in the 580 – 800 nm are ascribed to d-d transitions for the Ni(II) cations located

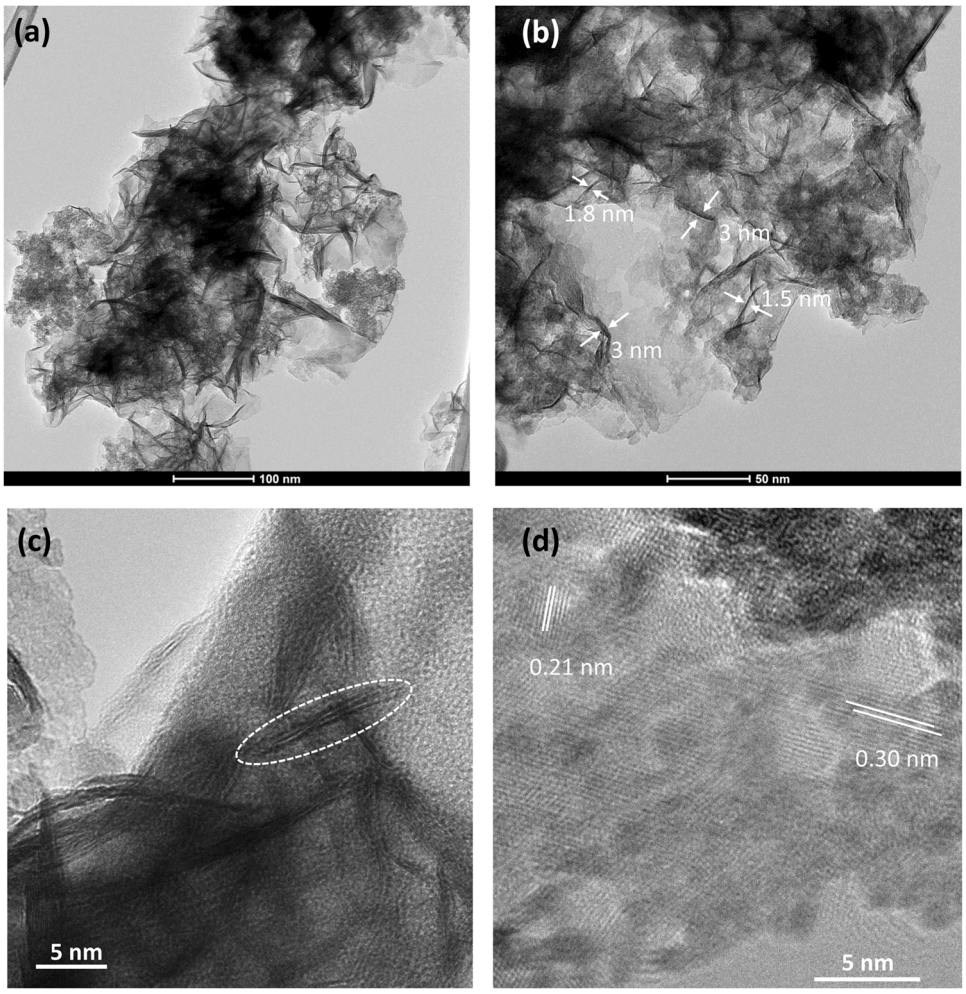

Fig. 3. HRTEM images of (a - c) NiTi-LDH and (d) GQDs/NiTi samples.

in the layers [33]. An increase in the absorbance of the visible light, mainly in the 380–550 nm range, is observed as the GQDs content is increased and associated to their light absorption ability (Fig. S2b). Additionally, the band gap values were estimated by the Kubelka-Munk method, Fig. 4d. In line with those previously reported [41,55] the presence of GQDs decreases the band gap from 2.97 to 2.86 and 2.83 eV, for NiTi-LDH, 1-GQDs/NiTi and 3-GQDs/NiTi, respectively. This decrease should be related with the increased electron density observed for Ti atoms in GQDs/NiTi samples (XPS results in Fig. 2). Accordingly, it is reported that 3d orbitals of Ti have influence in the conduction band minimum value [56]. From above, the sunlight harvesting is enhanced by the presence of GQDs, which may serve to boost the production of electron-hole pairs for photocatalytic reactions.

3.3. Photocatalytic activity

The ability of the samples to remove nitrogen oxide gases from air by means of a photocatalytic process was evaluated. Fig. 5a shows the variation of NO concentration measured during a standard test (500 ppb NO inlet concentration; 1 h UV-Vis light irradiation) for the NiTi-LDH and GQDs/NiTi samples used as photocatalysts. During a first period of 10 min in the dark, the inlet gas concentration remained strictly constant, indicating that no physical or chemical interaction between the gas reactant and catalyst or reactor accounts. Subsequently, once the samples are light irradiated (from 10th to 70th minute), a fast decay in the NO concentration measured values is observed. Therefore, a light induced process accounts for the photochemical oxidation (PCO) of NO molecules. As is known, the irradiation of a LDH semiconductor with the appropriate light promotes the transfer of electrons (e^-) from the valence band (VB) to the conduction band (CB) with the creation of holes (h^+) in the VB. This pair of charges (e^-/h^+), once they reach the photocatalyst's surface, initiate redox reactions on water and oxygen adsorbed molecules producing hydroxyl (·OH) and superoxide (O_2^-) radical species, which in term take part in the oxidation of nitrogen oxide gases. This photochemical process, even though it is quite complex [4–6], could be summarised in the following sequential oxidation steps: $NO \rightarrow NO_2^- \rightarrow NO_2 \rightarrow NO_3^-$.

The presence of GQDs enhances the photochemical De-NOx activity of the LDH, as can be deduced from the NO concentration profiles shown in Fig. 5a. Thus, under light irradiation, the NO removal efficiency increases from 55 % for the NiTi-LDH sample to 61 % for GQDs/NiTi samples. In addition, the decay of NO concentration values in the first few minutes of light irradiation is faster for the samples containing GQDs. In fact, the initial rate constants for NO degradation are higher in these samples (Fig. S7). Moreover, compared to the NiTi-LDH sample, the reached stationary state is completely constant with time during the irradiation period. In line with previous works, these observations are indicative that the addition of GQDs addition seems to enhance the electronic processes and, therefore, the De-NOx performance [41,57]. The NO and NOx conversion, NO_2 emission and selectivity values (%) measured for the three photocatalysts are shown in Fig. 5b. As is usual for LDH De-NOx photocatalysts [48,58–60], the released NO_2 is insignificant for NiTi-LDH (1.2 %) and GQDs/NiTi (< 0.6 %) samples. This is of high importance as the NO_2 intermediate product arising from the

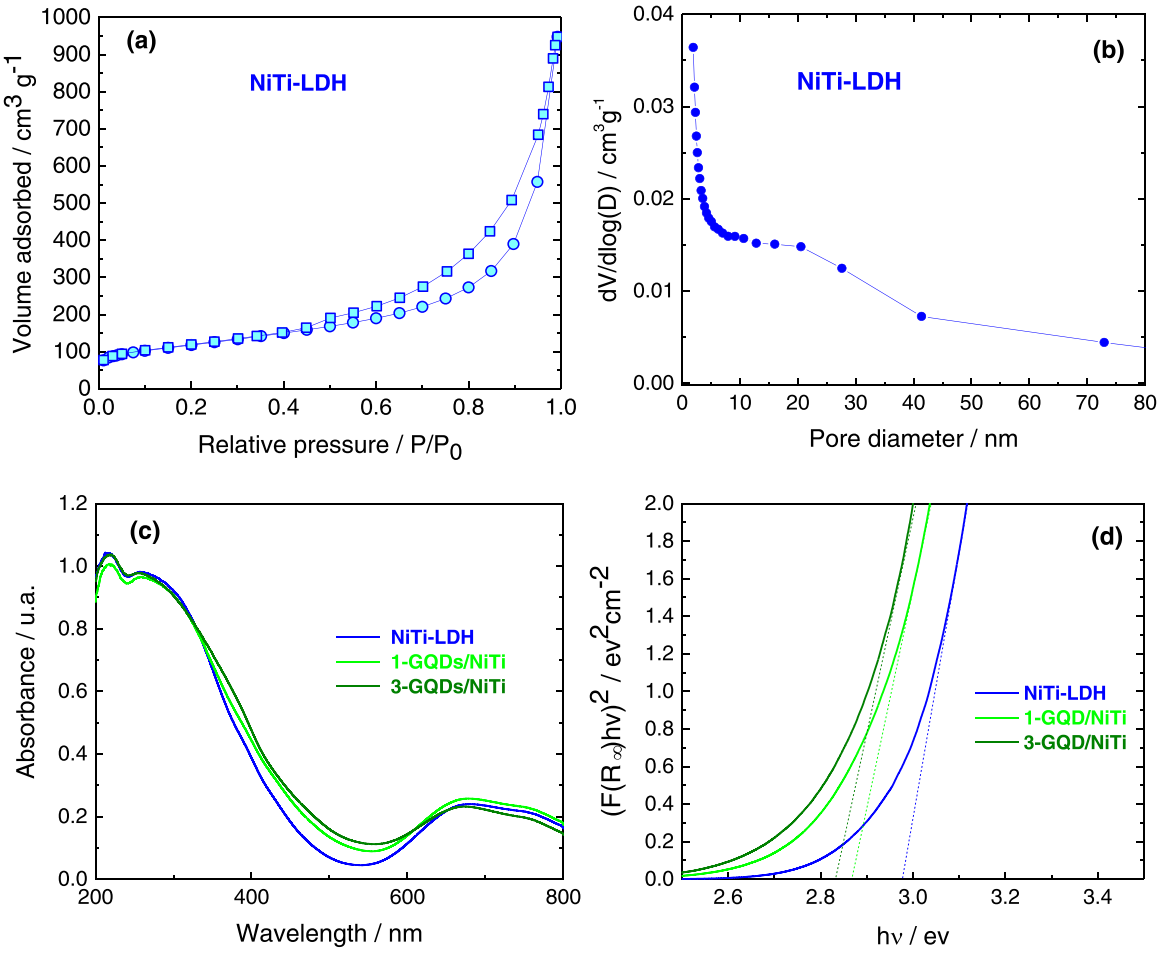

Fig. 4. (a) N_2 adsorption–desorption isotherms and (b) pore volume distribution for NiTi-LDH sample. (c) UV–Vis absorption spectra and (b) Kubelka-Munk transformed function plots for NiTi-LDH and GQDs/NiTi samples.

photochemical NO oxidation is considered a highly toxic product [61]. In this sense the De-NOx selectivity (S), defined as the amount of NO molecules removed from air as harmless nitrite/nitrate species, reaches outstanding values of 98 % for GQDs/NiTi. For comparison purposes, values corresponding to the TiO_2 P25 benchmark product (used as standard in this research field) were obtained under identical experimental conditions. Because of their high selectivity values, after one hour of light irradiation, the overall NOx removal efficiency exhibited by the GQDs/NiTi samples (60 %) clearly surpasses that for TiO_2 P25 (48 %), Fig. 5b. Considering both NOx and S efficiencies, the De-NOx performance of these photocatalysts are among the best values recently reported for advanced De-NOx photocatalysts, Table S1. Subsequently, the De-NOx experiments were repeated using visible light as the irradiation source (Fig. 5c). Clearly, the presence of GQDs promotes the visible light activity which should be associated with the better light harvesting (Figs. 4c and 4d) and/or an enhanced charge carrier separation in the system. The above results demonstrate that GQDs/NiTi samples can be successfully used for air purification purposes.

Interestingly, once the light is off (70^{th} minute), a different behaviour in the evolution of the NO concentration in the dark was observed for GQDs/NiTi samples. The NiTi-LDH sample exhibits the expected NO concentration values profile, Fig. 5d. Thus, in the absence of light irradiation, the photochemical process does not occur, and the NO values return to the initial values. However, the GQDs/NiTi samples showed a significant and prolonged post-photocatalytic NO removal, Figs. 5e and 5f. In fact, this process is clearly related to the amount of GQDs. Thus, a NO removal efficiency value in the dark, greater than 20 % (which means 100 ppb of NO removed) is sustained for 30 min, and 75 min in the case of 1-GQDs/NiTi for 3-GQDs/NiTi samples, respectively. Furthermore, the De-NOx behaviour in the dark was not dependent on the light irradiation period, as similar NO removal in the dark was observed after 10, 30 and 60 min of light irradiation, Fig S8. On the other hand, the stability of the sample after the catalytic tests was corroborated as no significative chemical nor morphological changes were found (Fig. S9). Compared to previous works, these results are a clear advance in post-photocatalytic De-NOx processes, as significant De-NOx ability (> 20 %) was previously reported to persist for only 8–10 min in the dark [7–10]. To gain information about the nature of the process observed on GQDs/NiTi samples in the dark period, additional studies were performed. Firstly, the massive adsorption of NO gas molecules on the surface of the photocatalyst was discarded because it was not observed during the first ten minutes of this De-NOx test. No nitrogen oxide adsorption was observed in additional experiments either, when the gas reactant was put in contact with the photocatalyst for a long time in the absence of light irradiation, Fig. S10. Therefore, an induced chemical process must be responsible for the NO removal in the dark period. Moreover, it is reasonable to consider the photoluminescence effect produced by GQDs under light irradiation as a new light activation process which should promote photochemical reactions once the light is off [62]. However, the photoluminescence signal emitted by GQDs persist only a few tens of nanoseconds in the absence of light, Fig S2d, thus indicating that a long-lasting activity of De-NOx in the dark is not due to the persistent luminescence. In addition, the temperature effect should be considered. In our experimental setup, the light irradiation box is air refrigerated to maintain a constant ambient temperature of 35 °C, but the continuous UV-Vis light fall on the sample

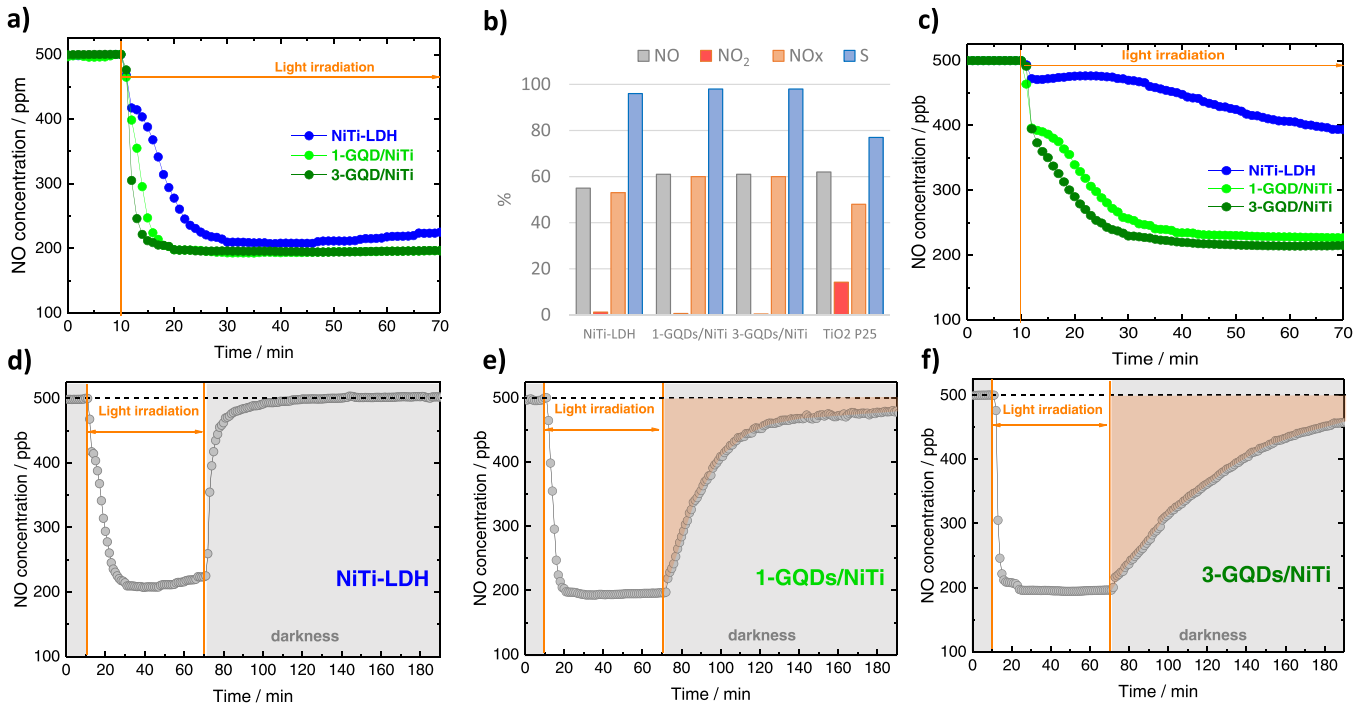

Fig. 5. (a) Gas concentration evolution during the photodegradation of NO under (a) UV-Vis or (c) visible light irradiation on NiTi-LDH and GQDs/NiTi samples. (b) NO conversion, NO_2 emitted, NOx conversion and selectivity values (%) for NiTi-LDH, GQDs/NiTi and TiO_2 P25 samples. (d - f) Gas concentration evolution during the catalytic reaction of NO in light/dark periods on NiTi-LDH and GQDs/NiTi samples.

increases the temperature to almost 60 °C on its surface, Fig. S11a. This temperature is that expected for a photocatalyst directly exposed to the sunlight, since roofs and walls of buildings – architectural elements on which De-NOx photocatalysts are applied – reach temperatures in the range of 55–61 °C under sunlight exposition [63]. To ascertain the effect of temperature on NO removal, the De-NOx process was performed in the dark while maintaining the reaction chamber at a constant temperature of 60 °C, Fig. S11b. It was observed that, in comparison to the photocatalytic experiment (Fig. 5), a very low NO removal efficiency of 15 % was obtained. However, once the heater is off, the NO abatement does not occur with temperatures lower than 40 °C. Both NiTi-LDH and 3-GQDs/NiTi samples exhibit a very similar behaviour. Figure S11a shows that the temperature of the sample surface decreases to 40 °C in only ten minutes once the light is off, but the NO abatement persists for 110 additional minutes. From these observations, it is concluded that a large persistent post-photocatalytic De-NOx process observed for the 3-GQDs/NiTi sample (Fig. 5f) is not promoted by temperature changes.

To confirm that the De-NOx process in the dark is a light induced process, an additional experiment was performed in which the photocatalyst was only exposed to the reactant NO gas in dark conditions. Previously, the photocatalysts were activated by UV-Vis light (1 h of light irradiation) before being placed in the reaction chamber. The corresponding NO gas concentration profile for NiTi-LDH and 3-GQDs/NiTi samples are shown in Fig. 6. In both cases, the samples were introduced into the reaction chamber after the first 20 min in which the NO flow was stabilised. Subsequently, the disruption of the NO values occurred because the reaction chamber was open to accommodate the sample. In the case of the NiTi-LDH sample, the disrupted inlet NO values were rapidly recovered in only a few minutes, indicating that no De-NOx process occurs in the dark. However, a significant NO removal (> 20 %) was preserved for at least one hour for the 3-GQDs/NiTi sample, confirming its ability to perform persistent photo-catalysis after light irradiation. As a control test, similar experiments were carried out with the standard TiO_2 P25 photocatalyst, with (3 wt%) and without GQDs (Fig. S12). Once the light was off, no post-photocatalytic process was observed as the NO concentration values were quickly

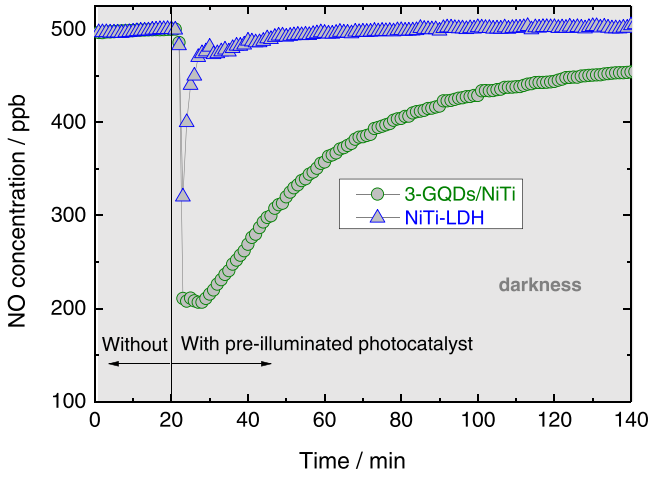

Fig. 6. NO gas concentration evolution in the dark on pre-illuminated NiTi-LDH and 3-GQDs/NiTi samples.

recovered for both samples. Therefore, the observed light-induced De-NOx process is not related to the individual systems (NiTi-LDH or GQDs), but to the actual GQDs/NiTi-LDH heterojunction. Finally, the light/dark catalytic process was repeated in different successive runs, Fig. S13. The same NO removal efficiency was found in both light and dark periods for the six runs indicating that the catalyst is not poisoned, and any chemical reaction accounted during the dark period should be reversible.

3.4. Photocatalytic mechanism assessment

Several experiments were performed to gain information about the plausible mechanism accounting under light and dark conditions. The ability of NiTi-LDH, under illumination, to produce ·OH and $O_2^{\cdot-}$ radicals was reported in our previous work [29]. These reactive oxygen species

(ROS) are responsible for initiating the redox processes. To get an insight into the photo-charge separation efficiency of the photocatalysts, pico-second time-resolved photoluminescence (TRPL) measurements were performed. Fig. 7a shows the time profiles obtained at λ_{exc} = 405 nm with the best bi-exponential fits for the GQDs and also mixed with the NiTi-LDH photocatalyst, leading to deactivation times equal to 10.3 ns (GQDs), 0.6 and 5.4 ns ($\tau_{av.}$ = 2.1 ns) for 1-GQDs/NiTi sample, 0.5 and 5.3 ns ($\tau_{av.}$ = 2.2 ns) for 3-GQDs/NiTi sample. The deactivation kinetics for the excited state in GQDs/NiTi-LDH samples is developed in a shorter time range compared with the GQDs sample. Furthermore, Fig. 7b compares the PL spectra of the NiTi-LDH, 3-GQDs/NiTi and GQDs samples (λ_{exc} = 350 nm). A large quenching of the GQD emission signal is observed when the GQDs are linked to the LDH structure, indicating a marked transfer of photoexcited electrons from GQDs to LDH. These observations, together with those from XPS measurements (Fig. 2) confirm the formation of an effective electronic heterojunction between GQDs and LDH, which is beneficial for the photocatalytic activity of these samples, as inferred from the De-NOx results (Fig. 5).

Additionally, in situ DRIFTS technique was used to perform the dynamic monitoring of the detailed mechanism involved in the photocatalytic removal of NO. Firstly, to remove environmental impurities, the samples were subjected to a pre-treatment process flowing the measurement cell with Ar for 10 min, and no IR spectral variations were found. The background spectrum was recorded before the reactant gas mixture (NO + O_2) flowed through the reaction chamber. Subsequently, and after 10 min of stabilisation in the dark, the samples were light irradiated for 30 min. The corresponding spectra obtained, once the background had been subtracted, for samples NiTi-LDH and 3-GQDs/NiTi at different periods of illumination, are shown in Fig. 8. When light interacts with the samples, photoexcited e^- and h^+ are generated on the surface of the photocatalyst and react with H_2O and O_2 to produce hydroxyl and superoxide radicals. These radicals initiate the photochemical oxidation of NO, as revealed by the IR signals corresponding to nitrite and nitrate species. The detailed band assignment is reported in Table S2, SI. The low intensity signal at 1392–1397 cm^{-1} shows the appearance of N_2O_4 as an intermediary in the oxidation process. In both samples, the appearance of the NO^- signal corresponds to the NO disproportionation in the presence of the hydroxyl LDH groups [64]. In the case of NiTi-LDH (Fig. 8a), after 10 min of light irradiation, the main signal corresponds to nitrite (1100 cm^{-1}). The transformation of nitrites into nitrates takes place as the irradiation time is prolonged (20 and 30 min). Now, the highest intense signal corresponds to nitrate (1063 cm^{-1}) and the growth of 1534–1507 cm^{-1} and 1322–1277 cm^{-1} signals are observed, all corresponding to bridge/bidentate nitrate species. Similar features were found in the spectra obtained for 3-GQDs/NiTi sample during the illumination period. In comparison to NiTi-LDH, the nitrate signals increase in intensity and those for bidentate/quelated nitrates (1066, 1461, 1534 and 1584 cm^{-1}) are clearly observed, indicating that monodentate NO_3^- species transformation into the more stable bidentate ones, is favoured. These findings match with the De-NOx efficiency results (Fig. 5). Thus, the 3-GQDs/NiTi photocatalyst promotes the complete NO oxidation to nitrate, which is related to a more efficient charge transfer (Fig. 7).

Afterwards when the light was off, interestingly, the evolution of IR signals in the dark was markedly different for NiTi-LDH and 3-GQDs/NiTi samples. In the absence of light, as NO gas interacts with the

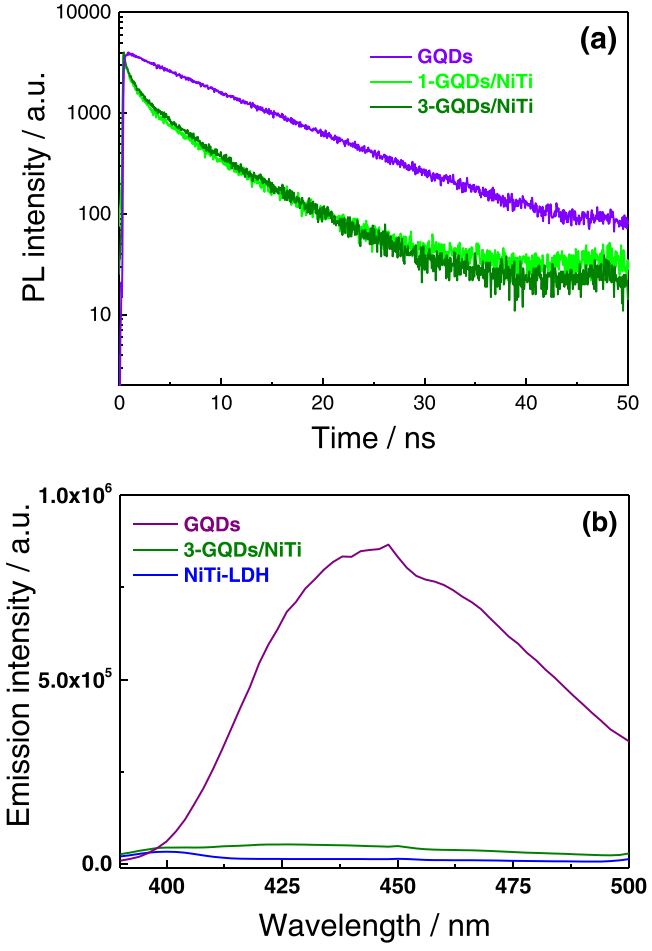

Fig. 7. (a) Time decay of the photoluminescence signals for GQDs and GQDs/NiTi samples. (b) PL spectra of GQDs, NiTi-LDH and 3-GQDs/NiTi samples.

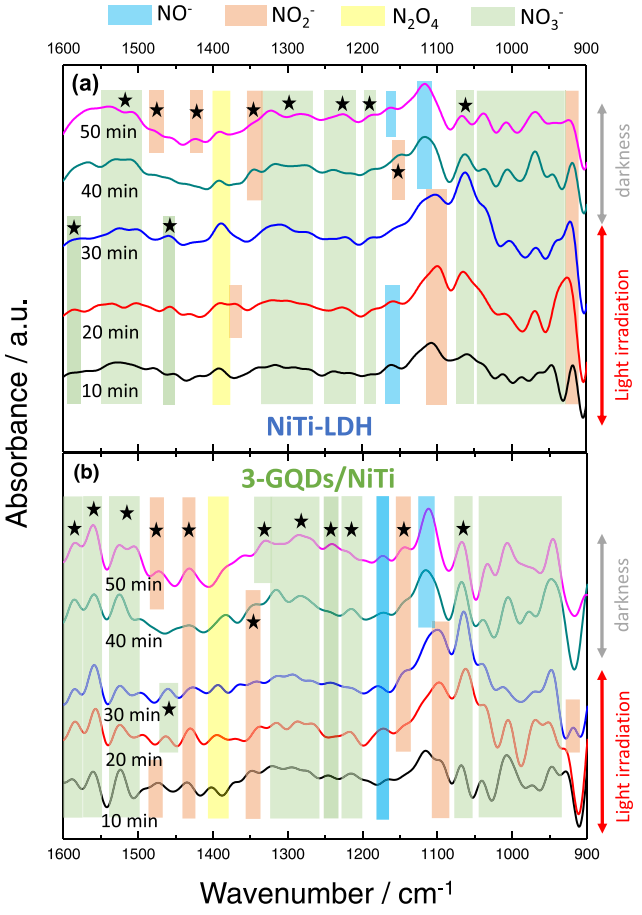

Fig. 8. *In situ* DRIFTS spectra obtained while NO and O_2 gases are flowing through the (a) NiTi-LDH and (b) 3-GQDs/NiTi samples under light and dark conditions.

surface of the NiTi-LDH sample (Fig. 8a), the main signal observed is that corresponding to NO^- (1116 cm^{-1}). In addition, signals of new nitrite species (1347, 1420 and 1476 cm^{-1}) are found together with a decrease in intensity for some of the nitrate signals, mainly those located at 1063 cm^{-1}. These findings indicate that, once the photochemical oxidation process has stopped, the reactions that occur on photocatalyst surface correspond to: (i) the NO disproportionation, ii) a renoxification process between NO as NO_3^-. A different evolution of the IR spectra is found for the 3-GQDs/NiTi sample (Fig. 8b). Even though the NO^- signal is again the highest in intensity, the decrease in intensity for the nitrate signal at 1063 cm^{-1} is now attenuated. Of importance, a significant increase in several nitrate signals (944, 1007, 1033, 1211–1327 and 1507 cm^{-1}) is observed. Therefore, the oxidation of NO gas molecules to nitrate species continues after the light is off, thus explaining the persistent post-photocatalytic De-NOx process observed for this sample (Fig. 5f).

In order to confirm the existence of the persistent catalytic process once the light is off, an additional DRIFTS experiment was performed. On this occasion, the 3-GQDs/NiTi sample was previously exposed to light irradiation under Ar atmosphere for one hour. Subsequently, the light was turned off and then the NO was flowed inside the reaction chamber. This means that NO interacts with the surface of the photocatalyst in the dark only when the sample was previously activated by light irradiation. Signals corresponding to nitrite and nitrate species are clearly observed again, Fig. 9, corroborating that NO oxidation occurs in the dark over the pre-irradiated 3-GQDs/NiTi sample. Now, several intense signals for nitrite species (906, 1341, 1438 and 1487 cm^{-1}) are registered, which indicates that catalytic reaction is less effective in the dark compared to that directly assisted by light. This is in accordance with the De-NOx performance observed for the 3-GQDs/NiTi sample for both light irradiation and dark periods (Fig. 5).

To explain the mechanism occurring in the dark, we assume that NiTi-LDH also acts as ESM material when GQDs/NiTi is light irradiated. As previously commented in the Introduction section, this assumption is based on the role played by graphene and Ti^{4+} cations in energy storage systems, as a source and drain of electrons, respectively [25,30,65,66]. The participation of electrons during the dark period was double checked. Firstly, EPR measurements were performed to prove the existence of reactive species which could be involved in the chemical reaction, using DMPO (5,5-Dimethyl-1-pyrroline N-oxide) for radical detection. Before EPR measurements, the 3-GQDs/NiTi sample was light irradiated for one hour. Subsequently, in the dark, the sample and DMPO were put in close contact and the corresponding EPR signals measured after 10 min. Fig. 10a shows that the DMPO-·OH adduct was not formed, but weak signals attributed to the DMPO-·O_2^- adduct. [48,67] were observed. This confirms that 3-GQDs/NiTi is supplying electrons to

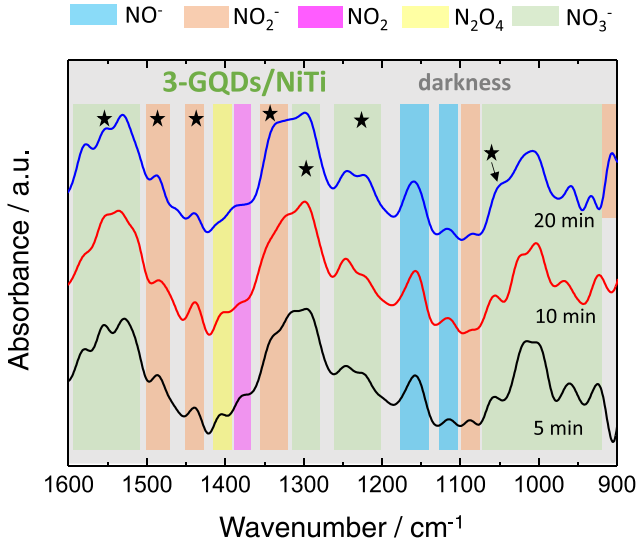

Fig. 9. *In situ* DRIFTS spectra obtained in the dark for the pre-illuminated 3-GQDs/NiTi sample.

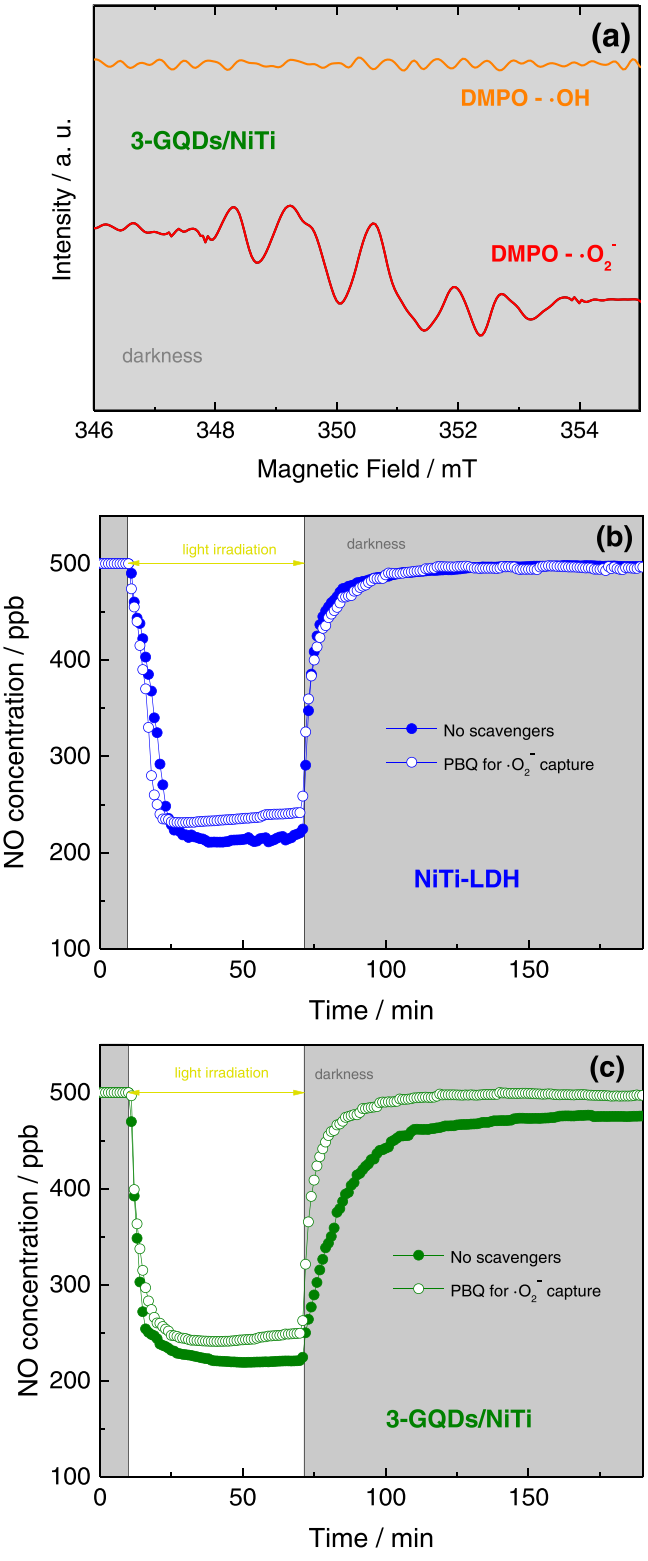

Fig. 10. (a) DMPO spin-trapping EPR spectra obtained in dark conditions for the pre-illuminated 3-GQDs/NiTi sample. Active species trapping experiments for the photocatalytic NO oxidation process over (b) NiTi-LDH and (c) 3-GQDs/NiTi sample.

the reaction medium. To corroborate this evidence, scavenger experiments using p-benzoquinone (PBQ) to trap superoxide anion radical species were carried out during De-NOx tests performed with NiTi-LDH and 3-GQDs/NiTi samples, Figs. 10b and 10c. For both photocatalysts, as expected, the presence of PBQ decreases the NO removal activity during the light irradiation period. In the dark period, PBQ only has influence in the NO signal recorded for the 3-GQDs/NiTi sample (Fig. 10c), indicating again that superoxide radicals are present in this period. Additionally, the use of $K_2Cr_2O_7$ scavenger shows that electrons also participate in the chemical reaction which takes place in the dark when 3-GQDs/NiTi is used as a photocatalyst, Fig. S14. With similarity to that reported for the TiO_2-Cu_2O storage material [25,30], titanium centres should be contemplated as the electron trap. Under light irradiation, Ti^{4+} would be partially reduced to Ti^{3+} due to the deep electron injection from excited GQDs nanoparticles, which explains the persistent post-photocatalytic De-NOx reaction in samples containing GQDs and its intensification when the amount of GQDs is increased. Because the Ti(IV) and Ti(III) ionic radius in octahedral coordination are different enough (68 and 79 pm, respectively [68]), the partial reduction of Ti(IV) should induce changes in the M−O−M bonds through the interconnected octahedra constituting the LDH layer. Thus, we studied the far-IR spectra of the 3-GQDs/NiTi sample using the in situ DRIFTS technique. Previously, the IR spectrum of the 3-GQDs/NiTi sample was recorded and used as a background spectrum. Fig. S15 shows the dynamic monitoring of the IR signal, once the background spectrum is subtracted, at different periods of light illumination and dark. Before the sample was irradiated, the signal measured in dark served as a baseline. Under light irradiation new bands appear, which are associated to changes in the vibration modes of Ti−O−Ti and Ni−O−Ni (460 and 483 cm^{-1}; [69–72]), δ_{OH} in-plane deformation (521 cm^{-1}; [71]), Ni−O (535 cm^{-1}; [72,73]) and Ti-O (560, 588 and 607 cm^{-1}; [69,70]) bonds. After 60 min of light illumination, the lamp was switched off and spectra were recorded in the dark. After 15 min in the dark, some M−O bands (535 cm^{-1}) tend to disappear and those corresponding to Ti−O−Ti and Ni−O−Ni bonds are slightly shifted to lower frequencies, indicating that the LDH layer is being rearranged. Finally, the new signals observed during the experiment are vanished after 30 min in the dark and, presumably, the pristine chemical identity of the 3-GQDs/NiTi sample is recovered, in accordance with the preserved De-NOx activity observed in the running tests shown in Fig. S13.

The results described above show that pre-illuminated GQDs/NiTi photocatalysts exhibit a catalytic memory thanks to the existence of stored electrons. The ability of Ti^{4+} to be photo-reduced in adequate heterojunctions together with the electron injection [69] assist this mechanism [25,30,65,74]. Moreover, the participation of electrons and superoxide radicals once the light is off, are both indicative that a simultaneous electron storage mechanism takes place in GQD/NiTi compound. Therefore, the complete De-NOx process for GQDs/NiTi photocatalysts in light/dark conditions should be assumed to occur by a combination of photocatalytic and energy storage mechanisms. In order to stablish the alignment of the energy bands for GQDs/NiTi photocatalyst, several measurements were performed. The Valence Band XPS spectrum was acquired for the NiTi-LDH, the valence band edge being 3.14 eV vs NHE (Fig. S16a). Therefore, by considering the previously obtained band gap value (2.97 eV), the conduction band edge is located at 0.17 eV. Meanwhile, the UPS spectrum of NiTi-LDH (Fig. S16b) allowed to locate the Fermi level at 1.3 eV from the valence band (p-type semiconductor). Furthermore, the GQDs band gap value was calculated to be 3.07 eV (Fig. S17a), whereas its Mott-Schottky plot showed a positive slope, indicating its n-type semiconductive behaviour (Fig. S17b). By extrapolating the linear region of the Mott-Schottky plot, the flat band potential can be estimated, and it can be considered as the conduction band value [36,37]. Considering all these results, the conduction band edge and the valence band edge of the GQDs were located at −0.38 eV and 2.69 eV vs NHE, respectively. Consequently, a p-n heterojunction between NiTi-LDH and GQDs is created. Fig. S18 represents the p-n heterojunction formed between NiTi-LDH and GQDs, a mechanism successfully used in previously reported works [75–78]. The photocatalysis mechanism is initiated once light photons are absorbed on the surface of NiTi-LDH nanosheets resulting in electron excitation to the CB, whereas holes are generated in the VB (Eq. 1). Simultaneously, because of the effective heterojunction formed between GQDs and NiTi-LDH, as inferred from the aforementioned XPS and PL results (Figs. 2 and 7), a charge transfer (electrons) from GQDs CB to NiTi-LDH CB is generated under irradiation, leading to an electron enrichment in NiTi-LDH. Similarly, the holes move from NiTi-LDH VB to GQDs VB. Thus, the e^-/h^+ recombination is retarded, increasing the photocatalytic De-NOx efficiency of GQDs/NiTi photocatalysts, mainly under Visible light irradiation (Fig. 5c). On the photocatalyst surface, the e^- and h^+ promote the formation of ROS species which initiate the oxidation of NO molecules towards nitrite/nitrate species, as was monitored by the DRIFTS technique (Fig. 8). This photo-oxidative De-NOx process involving several steps was previously reported by our group [29] and is now described in SI. Furthermore, in similitude with previous works [25,30], the following energy storage mechanisms should be considered. The occurrence of Ti^{3+} in NiTi LDH should be possible due to the GQD electron injection during the irradiation period (Eq. 2). Once the light is off, the stored electrons are released again (by $Ti^{3+} \rightarrow Ti^{4+}$ process) to the catalyst surface (Eq. 3) where they react with oxygen molecules to produce superoxide radicals (Eq. 4) (Fig. 10), the latter activating the De-NOx oxidative process in the dark.

$$NiTi + hv \rightarrow NiTi^* \ (e^-_{CB} + h^+_{VB}) \quad (1)$$

$$e^-_{CB}(GQD^*)NiTi^* \rightarrow NiTi^{4+}Ti^{3+} \quad (2)$$

$$NiTi^{4+}Ti^{3+} \rightarrow NiTi + e^- \quad (3)$$

$$e^- + O_2 \rightarrow \cdot O_2^- \quad (4)$$

This reversible catalytic mechanism could explain the good reusability of the catalyst in successive runs (Fig. S13).

4. Conclusions

GQDs/NiTi-LDH heterojunctions were synthesised with different amounts of graphene quantum dots. The incorporation of GQDs to the NiTi-LDH photocatalyst does not alter the morphological, chemical nor microstructural properties. GQDs nanoparticles are placed between NiTi-LDH nanosheets forming an efficient electronic heterojunction. The incorporation of GQDs enhance the light harvesting ability of the photocatalyst as the absorbance of the visible light is increased.

The beneficial effects of GQDs incorporation led to a better De-NOx response of GQDs/NiTi photocatalysts compared to NiTi-LDH, mainly under visible light. GQDs/NiTi photocatalysts are highly selective towards the NO photo-oxidation to nitrite/nitrate species and, therefore, exhibiting higher NOx gas abatement values than the standard TiO_2 P25 photocatalyst. Once the light is off, a great persistence of the catalytic process is observed in the dark for the GQDs/NiTi compounds. This process is dependent on the GQDs content in the heterojunction, but not on the illumination time nor the temperature reached by the photocatalyst during the light irradiation period. The similar De-NOx efficiency observed for all catalytic run tests performed in the dark is related to a chemical/electron reversible process.

The De-NOx process performed by GQDs/NiTi compounds in light/dark conditions is explained by the simultaneous occurrence of photocatalytic and energy storage mechanisms. Under light irradiation, the creation of charge carriers (e^- and h^+) promote the formation of ROS radical species which initiates the sequential $NO \rightarrow NO_2^- \rightarrow NO_2 \rightarrow NO_3^-$ oxidation process. Thanks to the formation of a p-n heterojunction between GQDs and NiTi-LDH, the photo-oxidative process is favoured in GQDs/NiTi compounds. Simultaneously, some of the excited electrons occurring during the light irradiation period are trapped and stored by

the NiTi-LDH. Once the light is off, the stored electrons are released again, favouring the formation of superoxide radicals which maintain the De-NOx process in the dark. We conclude that LDHs provide a new platform approach to develop new persistent photocatalytic systems with the aim to achieve day/night photocatalysis practical applications.

Declaration of Competing Interest

The authors declare that they have no known competing financial interests or personal relationships that could have appeared to influence the work reported in this paper.

Data availability

Data will be made available on request.

Acknowledgements

This work was partly financed by the FEDER 2014–2020 programme (Consejería de Economía, Conocimiento, Empresas y Universidad de la Junta de Andalucía; 1380752-R project), the P.O. FEDER ANDALUCÍA (2014–2020, Consejería de Transformación Económica, Industria, Conocimiento y Universidad, PY20_00365 project) and Agencia Estatal de Investigación (Spain; MCIN/AEI/10.13039/501100011033; MCIN PID2020–117516 GB-I00 and MCIN PID2020–117832RB-I00 projects). Javier Fragoso acknowledges a contract from the Spanish Government (PRE2018–084594).

CRediT authorship contribution statement

Javier Fragoso: Investigation, Data curation, Visualization. **Adrián Pastor:** Supervision, Investigation, Writing – reviewing and editing. **Manuel Cruz-Yusta:** Methodology, Investigation. **Francisco Martin:** Investigation. **Gustavo de Miguel:** Investigation. **Ivana Pavlovic:** Funding acquisition, Writing – reviewing and editing. **Mercedes Sánchez:** Investigation, Funding acquisition. **Luis Sánchez:** Conceptualisation, Project administration, Writing – reviewing and editing.

Appendix A. Supporting information

Supplementary data associated with this article can be found in the online version at doi:10.1016/j.apcatb.2022.122115.

References

[1] S. Rajendran, T.A.K. Priya, K.S. Khoo, T.K.A. Hoang, H.-S. Ng, H.S.H. Munawaroh, C. Karaman, Y. Orooji, P.L. Show, A critical review on various remediation approaches for heavy metal contaminants removal from contaminated soils, Chemosphere 287 (2022), 132369, https://doi.org/10.1016/j.chemosphere.2021.132369.

[2] B.H. Chen, C.J. Hong, H.D. Kan, Exposures and health outcomes from outdoor air pollutants in China, Toxicology 198 (2004) 291–300, https://doi.org/10.1016/j.tox.2004.02.005.

[3] European Environment Agency, Air quality in Europe-2019 report, 2019. ⟨https://doi.org/10.2800/822355⟩.

[4] J. Balbuena, M. Cruz-Yusta, L. Sánchez, Nanomaterials to combat NO_x pollution, J. Nanosci. Nanotechnol. 15 (2015) 6373–6385, https://doi.org/10.1166/jnn.2015.10871.

[5] M. Cruz-Yusta, M. Sánchez, L. Sánchez, Metal oxide nanomaterials for nitrogen oxides removal in urban environments, in: C. Maccato, D. Barreca (Eds.), Tailored Functional Oxide Nanomaterials: From Design to Multi-Purpose Applications, Wiley-VCH GmbH, 2022, pp. 229–276. ISBN-13: 978-3527347599; 10.1016/j.apsusc.2017.08.192.

[6] A. Nikokavoura, C. Trapalis, Graphene and g-C_3N_4 based photocatalysts for NO_x removal: a review, in: Appl. Surf. Sci., 430, 2018, pp. 18–52, https://doi.org/10.1016/j.apsusc.2017.08.192.

[7] H. Li, S. Yin, T. Sato, Novel luminescent photocatalytic deNO_x activity of $CaAl_2O_4$:(Eu,Nd)/$TiO_{2-x}N_y$ composite, Appl. Catal. B 106 (2011) 586–591, https://doi.org/10.1016/j.apcatb.2011.06.019.

[8] H. Li, S. Yin, Y. Wang, T. Sato, Efficient persistent photocatalytic decomposition of nitrogen monoxide over a fluorescence-assisted $CaAl_2O_4$:(Eu, Nd)/(Ta, N)-codoped TiO_2/Fe_2O_3, Appl. Catal. B. 132–133 (2013) 487–492, https://doi.org/10.1016/j.apcatb.2012.12.026.

[9] H. Li, S. Yin, Y. Wang, T. Sato, Microwave-assisted hydrothermal synthesis of Fe_2O_3-sensitized $SrTiO_3$ and its luminescent photocatalytic deNO_x activity with $CaAl_2O_4$:(Eu, Nd) assistance, J. Am. Ceram. Soc. 96 (2013) 1258–1262, https://doi.org/10.1111/jace.12206.

[10] H. Li, S. Yin, Y. Wang, T. Sekino, S.W. Lee, T. Sato, Roles of Cr^{3+} doping and oxygen vacancies in $SrTiO_3$ photocatalysts with high visible light activity for NO removal, J. Catal. 297 (2013) 65–69, https://doi.org/10.1016/j.jcat.2012.09.019.

[11] F. Kang, G. Sun, P. Boutinaud, H. Wu, F.-X. Ma, J. Lu, J. Gan, H. Bian, F. Gao, S. Xiao, Recent advances and prospects of persistent luminescent materials as inner secondary self-luminous light source for photocatalytic applications, Chem. Eng. J. 403 (2021), 126099, https://doi.org/10.1016/j.cej.2020.126099.

[12] M. Sakar, C.C. Nguyen, M.H. Vu, T.O. Do, Materials and mechanisms of photo-assisted chemical reactions under light and dark conditions: canday–night photocatalysis be achieved? ChemSusChem 11 (2018) 809–820, https://doi.org/10.1002/cssc.201702238.

[13] J.Y.Y. Loh, G. Sharma, N.P. Kherani, G.A. Ozin, Post-illumination photoconductivity enables extension of photo-catalysis after sunset, Adv. Energy Mater. 11 (2021) 2101566, https://doi.org/10.1002/aenm.202101566.

[14] N. Lakshminarasimhan, U. v Varadaraju, Luminescence and afterglow in Sr_2SiO_4:Eu^{2+}, RE^{3+} [RE=Ce, Nd, Sm and Dy] phosphors – role of co-dopants in search for afterglow, Mater. Res. Bull. 43 (2008) 2946–2953, https://doi.org/10.1016/j.materresbull.2007.12.005.

[15] D. Jia, R.S. Meltzer, W.M. Yen, W. Jia, X. Wang, Green phosphorescence of $CaAl_2O_4$:Tb^{3+},Ce^{3+} through persistence energy transfer, Appl. Phys. Lett. 80 (2002) 1535–1537, https://doi.org/10.1063/1.1456955.

[16] H. Guo, Y. Wang, W. Chen, W. Zeng, S. Han, G. Li, Y. Li, Controlling and revealing the trap distributions of Ca6BaP4O17:Eu2+,R3+ (R = Dy, Tb, Ce, Gd, Nd) by codoping different trivalent lanthanides, J. Mater. Chem. C 3 (2015) 11212–11218, https://doi.org/10.1039/C5TC02283E.

[17] J. Zhang, B. Chen, J. Sun, X. Li, L. Cheng, H. Zhong, White long-lasting phosphorescence generation in a $CaAl_2Si_2O8$:: Eu2+, Mn2+, Dy3+ system through persistent energy transfer, J. Phys. D. Appl. Phys. 45 (2012), 325105, https://doi.org/10.1088/0022-3727/45/32/325105.

[18] W. Chen, Y. Wang, W. Zeng, G. Li, H. Guo, Design, synthesis and characterization of near-infrared long persistent phosphors $Ca_4(PO_4)_2O$:Eu^{2+},R^{3+} (R = Lu, La, Gd, Ce, Tm, Y), RSC Adv. 6 (2016) 331–337, https://doi.org/10.1039/C5RA19762G.

[19] E. Uzun, E. Öztürk, N.K. Ozpozan, E. Karacaoglu, Thermoluminescence and photoluminescence properties of Mn^{4+}, $Pr^{3+,4+}$, Nd^{3+} and Eu^{3+} in $MgAl_2Si_2O_8$, J. Lumin. 173 (2016) 73–81, https://doi.org/10.1016/j.jlumin.2015.12.043.

[20] V. Castaing, A.D. Sontakke, A.J. Fernández-Carrión, N. Touati, L. Binet, M. Allix, D. Gourier, B. Viana, Persistent luminescence of $ZnGa_2O_4$:Cr^{3+} transparent glass ceramics: effects of excitation wavelength and excitation power, Eur. J. Inorg. Chem. 2017 (2017) 5114–5120, https://doi.org/10.1002/ejic.201700841.

[21] Y. Cong, Y. He, B. Dong, Y. Xiao, L. Wang, Long afterglow properties of Zn_2GeO_4:Mn^{2+}, Cr^{3+} phosphor, Opt. Mater. 42 (2015) 506–510, https://doi.org/10.1016/j.optmat.2015.01.045.

[22] T. Tatsuma, S. Saitoh, Y. Ohko, A. Fujishima, TiO_2−WO_3 photoelectrochemical anticorrosion system with an energy storage ability, Chem. Mater. 13 (2001) 2838–2842, https://doi.org/10.1021/cm010024k.

[23] T. Tatsuma, S. Saitoh, P. Ngaotrakanwiwat, Y. Ohko, A. Fujishima, Energy storage of TiO_2−WO_3 photocatalysis systems in the gas phase, Langmuir 18 (2002) 7777–7779, https://doi.org/10.1021/la026011i.

[24] Y. Takahashi, T. Tatsuma, Oxidative energy storage ability of a TiO_2−$Ni(OH)_2$ bilayer photocatalyst, Langmuir 21 (2005) 12357–12361, https://doi.org/10.1021/la052107b.

[25] L. Xiong, M. Ouyang, L. Yan, J. Li, M. Qiu, Y. Yu, Visible-light energy storage by Ti^{3+} in TiO_2/Cu_2O bilayer film, Chem. Lett. 38 (2009) 1154–1155, https://doi.org/10.1246/cl.2009.1154.

[26] Y. Takahashi, T. Tatsuma, Visible light-induced photocatalysts with reductive energy storage abilities, Electrochem. Commun. 10 (2008) 1404–1407, https://doi.org/10.1016/j.elecom.2008.07.026.

[27] Q. Li, Y.W. Li, P. Wu, R. Xie, J.K. Shang, Palladium oxide nanoparticles on nitrogen-doped titanium oxide: accelerated photocatalytic disinfection and post-illumination catalytic "memory, Adv. Mater. 20 (2008) 3717–3723, https://doi.org/10.1002/adma.200800685.

[28] Q. Zhang, H. Wang, Z. Li, C. Geng, J. Leng, Metal-free photocatalyst with visible-light-driven post-illumination catalytic memory, ACS Appl. Mater. Interfaces 9 (2017) 21738–21746, https://doi.org/10.1021/acsami.7b02473.

[29] A. Pastor, C. Chen, G. de Miguel, F. Martin, M. Cruz-Yusta, J.C. Buffet, D. O'Hare, I. Pavlovic, L. Sánchez, Aqueous miscible organic solvent treated NiTi layered double hydroxide De-NO_x photocatalysts, Chem. Eng. J. 429 (2022), 132361, https://doi.org/10.1016/j.cej.2021.132361.

[30] L. Liu, W. Yang, Q. Li, S. Gao, J.K. Shang, Synthesis of Cu2O nanospheres decorated with TiO_2 nanoislands, their enhanced photoactivity and stability under visible light illumination, and their post-illumination catalytic memory, ACS Appl. Mater. Interfaces 6 (2014) 5629–5639, https://doi.org/10.1021/am500131b.

[31] J.P. Yasomanee, J. Bandara, Multi-electron storage of photoenergy using Cu_2O–TiO_2 thin film photocatalyst, Sol. Energy Mater. Sol. Cells 92 (2008) 348–352, https://doi.org/10.1016/j.solmat.2007.09.016.

[32] Y. Gu, Z. Lu, Z. Chang, J. Liu, X. Lei, Y. Li, X. Sun, NiTi layered double hydroxide thin films for advanced pseudocapacitor electrodes, J. Mater. Chem. A. 1 (2013) 10655–10661, https://doi.org/10.1039/C3TA10954B.

[33] Y. Zhao, P. Chen, B. Zhang, D.S. Su, S. Zhang, L. Tian, J. Lu, Z. Li, X. Cao, B. Wang, M. Wei, D.G. Evans, X. Duan, Highly dispersed TiO_6 units in a layered double

hydroxide for water splitting, Chem. Eur. J. 18 (2012) 11949–11958, https://doi.org/10.1002/chem.201201065.
[34] C. Cheng, Q. Liang, M. Yan, Z. Liu, Q. He, T. Wu, S. Luo, Y. Pan, C. Zhao, Y. Liu, Advances in preparation, mechanism and applications of graphene quantum dots/semiconductor composite photocatalysts: a review, J. Hazard Mater. 424 (2022), 127721, https://doi.org/10.1016/j.jhazmat.2021.127721.
[35] J. Qian, J. Yan, C. Shen, F. Xi, X. Dong, J. Liu, Graphene quantum dots-assisted exfoliation of graphitic carbon nitride to prepare metal-free zero-dimensional/two-dimensional composite photocatalysts, J. Mater. Sci. 53 (2018) 12103–12114, https://doi.org/10.1007/s10853-018-2509-8.
[36] J. Qian, C. Shen, J. Yan, F. Xi, X. Dong, J. Liu, Tailoring the electronic properties of graphene quantum dots by P doping and their enhanced performance in metal-free composite photocatalyst, J. Phys. Chem. C 122 (2018) 349–358, https://doi.org/10.1021/acs.jpcc.7b08702.
[37] A. Yuan, H. Lei, F. Xi, J. Liu, L. Qin, Z. Chen, X. Dong, Graphene quantum dots decorated graphitic carbon nitride nanorods for photocatalytic removal of antibiotics, J. Colloid Interface Sci. 548 (2019) 56–65, https://doi.org/10.1016/j.jcis.2019.04.027.
[38] Y. Huang, Y. Liang, Y. Rao, D. Zhu, J. Cao, Z. Shen, W. Ho, S.C. Lee, Environment-friendly carbon quantum dots/$ZnFe_2O_4$ photocatalysts: characterization, biocompatibility, and mechanisms for NO removal, Environ. Sci. Technol. 51 (2017) 2924–2933, https://doi.org/10.1021/acs.est.6b04460.
[39] X. Li, H. Shi, T. Wang, Y. Zhang, S. Zuo, S. Luo, C. Yao, Photocatalytic removal of NO by Z-scheme mineral based heterojunction intermediated by carbon quantum dots, Appl. Surf. Sci. 456 (2018) 835–844, https://doi.org/10.1016/j.apsusc.2018.06.133.
[40] Y. Huang, Y. Gao, Q. Zhang, Y. Zhang, J. Cao, W. Ho, S.C. Lee, Biocompatible FeOOH-carbon quantum dots nanocomposites for gaseous NO_x removal under visible light: Improved charge separation and High selectivity, J. Hazard. Mater. 354 (2018) 54–62, https://doi.org/10.1016/j.jhazmat.2018.04.071.
[41] Y. Cui, T. Wang, J. Liu, L. Hu, Q. Nie, Z. Tan, H. Yu, Enhanced solar photocatalytic degradation of nitric oxide using graphene quantum dots/bismuth tungstate composite catalysts, Chem. Eng. J. 420 (2021), 129595, https://doi.org/10.1016/j.cej.2021.129595.
[42] Y. Ou, G. Zhu, F. Rao, J. Gao, J. Chang, X. Xie, W. Zhang, Y. Huang, M. Hojamberdiev, Coral-shaped $TiO_{2-\delta}$ decorated with carbon quantum dots and carbon nanotubes for NO removal, ACS Appl. Nano Mater. 4 (2021) 7330–7342, https://doi.org/10.1021/acsanm.1c01306.
[43] J. Liu, R. Li, B. Yang, Carbon dots: a new type of carbon-based nanomaterial with wide applications, ACS Cent. Sci. 6 (2020) 2179–2195, https://doi.org/10.1021/acscentsci.0c01306.
[44] S.K. Pal, Versatile photoluminescence from graphene and its derivatives, Carbon 88 (2015) 86–112, https://doi.org/10.1016/j.carbon.2015.02.035.
[45] Q. Wang, D. O'Hare, Large-scale synthesis of highly dispersed layered double hydroxide powders containing delaminated single layer nanosheets, Chem. Commun. 49 (2013) 6301–6303, https://doi.org/10.1039/C3CC42918K.
[46] U. Costantino, F. Marmottini, M. Nocchetti, R. Vivani, New synthetic routes to hydrotalcite-like compounds – characterisation and properties of the obtained materials, Eur. J. Inorg. Chem. 1998 (1998) 1439–1446, https://doi.org/10.1002/(SICI)1099-0682(199810)1998:10<1439::AID-EJIC1439>3.0.CO;2-1.
[47] C. Chen, M. Yang, Q. Wang, J.-C. Buffet, D. O'Hare, Synthesis and characterisation of aqueous miscible organic-layered double hydroxides, J. Mater. Chem. A 2 (2014) 15102–15110, https://doi.org/10.1039/C4TA02277G.
[48] J. Fragoso, M.A. Oliva, L. Camacho, M. Cruz-Yusta, G. de Miguel, F. Martin, A. Pastor, I. Pavlovic, L. Sánchez, Insight into the role of copper in the promoted photocatalytic removal of NO using $Zn_{2-x}Cu_xCr\text{-}CO_3$ layered double hydroxide, Chemosphere 275 (2021), 130030, https://doi.org/10.1016/j.chemosphere.2021.130030.
[49] M.C. Capel-Sanchez, G. Blanco-Brieva, J.M. Campos-Martin, M.P. de Frutos, W. Wen, J.A. Rodriguez, J.L.G. Fierro, Grafting strategy to develop single site titanium on an amorphous silica surface, Langmuir 25 (2009) 7148–7155, https://doi.org/10.1021/la900578u.
[50] M.C. Biesinger, L.W.M. Lau, A.R. Gerson, R.St.C. Smart, The role of the Auger parameter in XPS studies of nickel metal, halides and oxides, Phys. Chem. Chem. Phys. 14 (2012) 2434–2442, https://doi.org/10.1039/C2CP22419D.
[51] H. Yoon, D. Kim, M. Park, J. Kim, J. Kim, W. Sriturravanich, B. Shin, Y. Jung, S. Jeon, Extraordinary enhancement of UV absorption in TiO_2 nanoparticles enabled by low-oxidized graphene nanodots, J. Phys. Chem. C 122 (2018) 12114–12121, https://doi.org/10.1021/acs.jpcc.8b03329.
[52] X. Lv, J. Zhang, X. Dong, J. Pan, W. Zhang, W. Wang, G. Jiang, F. Dong, Layered double hydroxide nanosheets as efficient photocatalysts for NO removal: band structure engineering and surface hydroxyl ions activation, Appl. Catal. B 277 (2020), 119200, https://doi.org/10.1016/j.apcatb.2020.119200.
[53] C. Chen, A. Wangriya, J.C. Buffet, D. O'Hare, Tuneable ultra high specific surface area Mg/Al-CO_3 layered double hydroxides, Dalton Trans. 44 (2015) 16392–16398, https://doi.org/10.1039/C5DT02641E.
[54] Y. Zhao, Q. Wang, T. Bian, H. Yu, H. Fan, C. Zhou, L.-Z. Wu, C.-H. Tung, D. O'Hare, T. Zhang, Ni^{3+} doped monolayer layered double hydroxide nanosheets as efficient electrodes for supercapacitors, Nanoscale 7 (2015) 7168–7173, https://doi.org/10.1039/C5NR01320H.
[55] A. Qu, H. Xie, X. Xu, Y. Zhang, S. Wen, Y. Cui, High quantum yield graphene quantum dots decorated TiO_2 nanotubes for enhancing photocatalytic activity, Appl. Surf. Sci. 375 (2016) 230–241, https://doi.org/10.1016/j.apsusc.2016.03.077.
[56] Y. Zhao, B. Li, Q. Wang, W. Gao, C.J. Wang, M. Wei, D.G. Evans, X. Duan, D. O'Hare, NiTi-layered double hydroxides nanosheets as efficient photocatalysts for oxygen evolution from water using visible light, Chem. Sci. 5 (2014) 951–958, https://doi.org/10.1039/C3SC52546E.
[57] Y. Liu, S. Yu, Z. Zhao, F. Dong, X.A. Dong, Y. Zhou, N-doped $Bi_2O_2CO_3$/graphene quantum dot composite photocatalyst: enhanced visible-light photocatalytic NO oxidation and in situ DRIFTS studies, J. Phys. Chem. C 121 (2017) 12168–12177, https://doi.org/10.1021/acs.jpcc.7b02285.
[58] A. Pastor, F. Rodriguez-Rivas, G. de Miguel, M. Cruz-Yusta, F. Martin, I. Pavlovic, L. Sanchez, Effects of $Fe3^+$ substitution on Zn-Al layered double hydroxides for enhanced NO photochemical abatement, Chem. Eng. J. 387 (2020), https://doi.org/10.1016/j.cej.2020.124110.
[59] F. Rodriguez-Rivas, A. Pastor, C. Barriga, M. Cruz-Yusta, L. Sanchez, I. Pavlovic, Zn-Al layered double hydroxides as efficient photocatalysts for NO_x abatement, Chem. Eng. J. 346 (2018) 151–158, https://doi.org/10.1016/j.cej.2018.04.022.
[60] F. Rodriguez-Rivas, A. Pastor, G. de Miguel, M. Cruz-Yusta, I. Pavlovic, L. Sanchez, Cr^{3+} substituted Zn-Al layered double hydroxides as UV-Vis light photocatalysts for NO gas removal from the urban environment, Sci. Total Environ. 706 (2020), https://doi.org/10.1016/j.scitotenv.2019.136009.
[61] J.R. Balmes, M.D. Eisner, Chapter 74 – Indoor and outdoor air pollution, in: V. C. Broaddus, R.J. Mason, J.D. Ernst, T.E. King, S.C. Lazarus, J.F. Murray, J. A. Nadel, A.S. Slutsky, M.B. Gotway (Eds.), Murray and Nadel's Textbook of Respiratory Medicine, sixth ed., W.B. Saunders, Philadelphia, 2016, pp. 1331–1342, https://doi.org/10.1016/B978-1-4557-3383-5.00074-9.
[62] J. Fan, D. Li, X. Wang, Effect of modified graphene quantum dots on photocatalytic degradation property, Diam. Relat. Mater. 69 (2016) 81–85, https://doi.org/10.1016/j.diamond.2016.07.008.
[63] K.H. Kwak, J.J. Baik, Diurnal variation of NO_x and ozone exchange between a street canyon and the overlying air, Atmos. Environ. 86 (2014) 120–128, https://doi.org/10.1016/j.atmosenv.2013.12.029.
[64] J. Liao, W. Cui, J. Li, J. Sheng, H. Wang, X. Dong, P. Chen, G. Jiang, Z. Wang, F. Dong, Nitrogen defect structure and NO+ intermediate promoted photocatalytic NO removal on H_2 treated g-C_3N_4, Chem. Eng. J. 379 (2020), https://doi.org/10.1016/j.cej.2019.122282.
[65] K.J. Williams, C.A. Nelson, X. Yan, L.S. Li, X. Zhu, Hot electron injection from graphene quantum dots to TiO_2, ACS Nano 7 (2013) 1388–1394, https://doi.org/10.1021/nn305080c.
[66] P. Sudhagar, I. Herraiz-Cardona, H. Park, T. Song, S.H. Noh, S. Gimenez, I.M. Sero, F. Fabregat-Santiago, J. Bisquert, C. Terashima, U. Paik, Y.S. Kang, A. Fujishima, T. H. Han, Exploring graphene quantum dots/TiO_2 interface in photoelectrochemical reactions: solar to fuel conversion, Electrochim. Acta 187 (2016) 249–255, https://doi.org/10.1016/j.electacta.2015.11.048.
[67] A. Nehdi, N. Frini-Srasra, G. de Miguel, I. Pavlovic, L. Sánchez, J. Fragoso, Use of LDH- chromate adsorption co-product as an air purification photocatalyst, Chemosphere 286 (2022), 131812, https://doi.org/10.1016/j.chemosphere.2021.131812.
[68] N.N. Greenwood, A. Earnshaw. Chemistry of Elements, second ed., Butterworth-Heinemann, Oxford, 1997.
[69] T. López, E. Ortiz, R. Gómez, M. Picquart, Amorphous sol-gel titania modified with heteropolyacids, J. Solgel Sci. Technol. 37 (2006) 189–193, https://doi.org/10.1007/s10971-005-6627-9.
[70] A. Larbot, I. Laaziz, J. Marignan, J.F. Quinson, Porous texture of a titanium oxide gel: evolution as a function of medium used, J. Non-Cryst. Solids 147–148 (1992) 157–161, https://doi.org/10.1016/S0022-3093(05)80610-6.
[71] P. Oliva, J. Leonardi, J.F. Laurent, C. Delmas, J.J. Braconnier, M. Figlarz, F. Fievet, A. de Guibert, Review of the structure and the electrochemistry of nickel hydroxides and oxy-hydroxides, J. Power Sources 8 (1982) 229–255, https://doi.org/10.1016/0378-7753(82)80057-8.
[72] P.C. Yu, G. Nazri, C.M. Lampert, Spectroscopic and electrochemical studies of electrochromic hydrated nickel oxide films, Sol. Energy Mater. 16 (1987) 1–17, https://doi.org/10.1016/0165-1633(87)90003-7.
[73] A. Claude, V. Vaithianathan, R. Bairava Ganesh, R. Sathyalakshmi, P. Ramasamy, Growth and characterization of novel (Ni^{3+}, Mg^{2+}) bimetallic crystals of ammonium Di hydrogen phosphate, J. Appl. Sci. 6 (2006) 85–89. ⟨https://doi.org/10.3923/jas.2006.85.89⟩.
[74] R. Long, D. Casanova, W.-H. Fang, O.V. Prezhdo, Donor–acceptor interaction determines the mechanism of photoinduced electron injection from graphene quantum dots into TiO_2: π-stacking supersedes covalent bonding, J. Am. Chem. Soc. 139 (2017) 2619–2629, https://doi.org/10.1021/jacs.6b09598.
[75] Z. Guo, H. Wu, M. Li, T. Tang, J. Wen, X. Li, Phosphorus-doped graphene quantum dots loaded on TiO_2 for enhanced photodegradation, Appl. Surf. Sci. 526 (2020), 146724, https://doi.org/10.1016/j.apsusc.2020.146724.
[76] S. Kumar, A. Dhiman, P. Sudhagar, V. Krishnan, ZnO-graphene quantum dots heterojunctions for natural sunlight-driven photocatalytic environmental remediation, Appl. Surf. Sci. 447 (2018) 802–815, https://doi.org/10.1016/j.apsusc.2018.04.045.
[77] D. Pan, J. Jiao, Z. Li, Y. Guo, C. Feng, Y. Liu, L. Wang, M. Wu, Efficient separation of electron–hole pairs in graphene quantum dots by TiO_2 heterojunctions for dye degradation, ACS Sustain. Chem. Eng. 3 (2015) 2405–2413, https://doi.org/10.1021/acssuschemeng.5b00771.
[78] A. Raghavan, S. Sarkar, L.R. Nagappagari, S. Bojja, S. MuthukondaVenkatakrishnan, S. Ghosh, Decoration of graphene quantum dots on TiO_2 nanostructures: photosensitizer and cocatalyst role for enhanced hydrogen generation, Ind. Eng. Chem. Res. 59 (2020) 13060–13068, https://doi.org/10.1021/acs.iecr.0c01663.